eJSSNT Regular Paper

e-Journal of Surface Science and Nanotechnology **24**, 26–32 (2026)

Effect of Water Vapor in Thermal Diffusion of Indium into ZnO Nanoparticles

Halim Md Abdul,[a, †] Toshiyuki Yoshida,[b, ‡] Yasuhisa Fujita [b]

[a] *Graduate School of Natural Science and Technology, Shimane University, Matsue 690-8504, Japan*
[b] *Institute of Science and Engineering, Shimane University, Matsue 690-8504, Japan*
[†] *Corresponding author: halimabdul552@gmail.com*
[‡] *Corresponding author: yosisi@riko.shimane-u.ac.jp*

Received: 28 October, 2025; Accepted: 10 February, 2026; J-STAGE Advance Publication: 7 March, 2026; Published: 7 March, 2026

Thermal diffusion of indium (In) into ZnO nanoparticles (NPs) were examined to decrease sheet resistance values of ZnO NP layers sprayed on quartz substrates. NP layers made of as-synthesized ZnO NPs exhibited extremely high sheet resistance values. On the other hand, NP layers made of ZnO NPs with In diffusion, the sheet resistance showed large variation, and in particular, it decreased significantly showing a strong correlation with the water vapor contents in the gases during thermal diffusion. The sheet resistance value decreased down to the order of $10^5\ \Omega\ \mathrm{sq}^{-1}$ (minimum value of $6 \times 10^5\ \Omega\ \mathrm{sq}^{-1}$). From X-ray diffraction, energy dispersive X-ray spectroscopy and photoluminescence analyses, the effects of the surface defects of ZnO NPs and the ambient water vapor in thermal diffusion process were discussed.

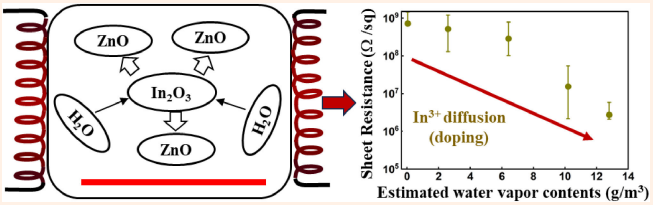

Keywords *ZnO nanoparticles; Indium doping; Thermal diffusion; Ambient effect; Water vapor effect*

I. INTRODUCTION

Semiconductor thin films and their interface controlling technologies are rapidly advancing and are supported by many cutting-edge technologies to provide high performance with high carrier conduction and well-behaved field effect properties and so on [1]. Many devices have evolved with these thin film technologies and will continue to proceed in the future. On the other hand, problems have become apparent, such as the rising process costs and the limitation of substrates being compatible with the film material. To overcome these issues, semiconductor "particle layers" have attracted attention due to their low cost, ease of use, large area compatibility, and above all, their versatility with greatly expanding the range of substrate options [2]. These features are important to expand the application field of semiconductor device technology, allowing new materials to be selected as substrates that were not previously possible in conventional thin film technologies. A lot of interests in utilizing semiconductor particle layers and coating techniques to produce thin-film-transistor (TFT) channel layers are reported [3, 4]. It is also important to be able to obtain particle layers in atmospheric- and solution-based processes. For this purpose, the use of oxide semiconductors is effective means to avoid insulation of particle surfaces by oxidation in air and/or water [5]. ZnO is one of promising oxide semiconductors due to its application in numerous fields, including optics [6], light-emitting diodes [7], thin-film transistor [8], and so on.

Particle layers have many benefits, however they also have significant disadvantages that restrict how well they work in electronic devices such as ZnO-particle-based TFTs. Because of the naturally loose organization of the particles, structural instability is one of the main problems. The existence of flaws in the particle layer is another important problem. Furthermore, the smooth passage of charge carriers is impeded by possible obstacles at the boundaries between individual particles. These features make the particle layer less effective for applications that need high-speed or high-conductivity performance since it shows less ability to flow current.

From the viewpoint of improving current transporting ability by reducing the sheet resistance of each ZnO particle, increasing carrier density by doping impurities into ZnO NPs is effective. This paper focuses on this point, and the thermal diffusion technique is attempted. Numerous parameters, including the size and form of the nanoparticles (NPs), the

concentration and distribution of defects, the temperature and duration of the diffusion process, might influence the thermal diffusion of III-group atoms, such as indium (In) [9], gallium (Ga) [10], and aluminum (Al) [11] into ZnO particles. Many attempts have been made in our laboratory using Ga_2O_3 as a Ga source to dope with ZnO particles to reduce the sheet resistance of obtained particle layers, but reliable TFT operation has not been achieved yet. One smart way to design and improve the characteristics of ZnO particle layers for a range of technological applications is to dope In. In is expected to be substituted to Zn, and the ionic radius of In (0.62 Å) is closer to that of Zn (0.60 Å) comparing with Ga (0.47 Å). ZnO is typically an n-type semiconductor, primarily because of intrinsic donor-related defects like zinc interstitials (Zn_i) and oxygen vacancies (V_O). In diffusion further improves conductivity because In^{3+} can replace Zn^{2+} in the ZnO lattice, creating more donor states and raising the density of conduction electrons. Consequently, by boosting carrier concentration and enhancing electron transport, In doping lowers the electrical resistance of ZnO films.

In this study, the effect of In doping into ZnO NPs by thermal diffusion was examined, in the viewpoint of lowering the sheet resistance of NP-layers. Since humidity-related adsorption modifies surface chemistry and defect charge states, which directly impact carrier transport and sheet resistivity, humidity is a significant external factor for ZnO-based films. Additionally, defect passivation and dopant diffusion behavior can be affected by humid atmospheres during annealing. Thus, studying humidity-dependent resistivity advances the creation of environmentally stable ZnO and offers mechanistic insight, when using thin-film devices. The low-cost compatible atmospheric spraying method was performed to obtain ZnO NP layers. Scanning electron microscopy (SEM), energy dispersive X-ray spectroscopy (EDS), X-ray diffraction (XRD), and photoluminescence (PL) spectroscopy were performed for evaluations.

II. EXPERIMENTAL METHOD

Gas evaporation mediated by arc discharge was used for the synthesis of ZnO NPs. Figure 1 illustrates the vertical arrangement of the free burning arc discharge experimental setup, while the specifics of the NPs synthesis process are briefly detailed in Ref. 12. Commercial metal zinc (4N, Nilaco) was used as anode, and a carbon rod was used as cathode. A rotary vacuum pump was used to maintain the chamber pressure of roughly 610 Torr while arc discharge at an arc current of 30 A was used to create ZnO NPs. ZnO NPs with n-type conduction can be obtained with dry air at a rate of 5 L min^{-1}. After the process, the chamber was allowed to cool to room temperature before opening. ZnO NPs were collected from the inner chamber walls, collection plate, and nearby surfaces around the growth zone. The deposited NPs were gently scraped using a clean spatula and transferred into a glass vial.

For the thermal diffusion of In, 0.06 g of In_2O_3 (Kojundo Chemical Laboratory) as an In source and 0.2 g of ZnO NPs

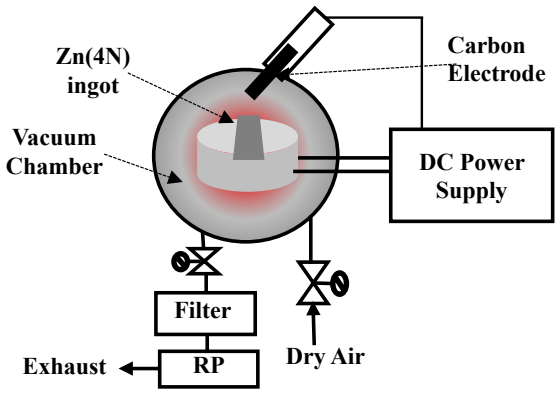

Figure 1: Illustration of the arc-discharge-mediated gas-evaporation method used for ZnO NP synthesis.

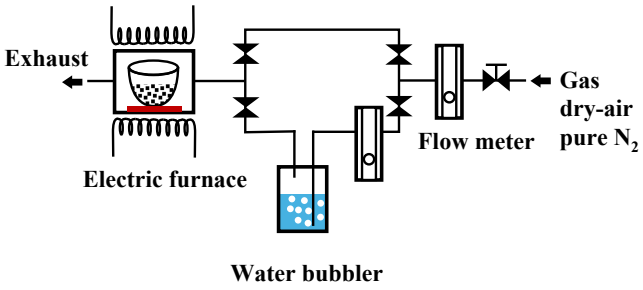

Figure 2: Illustrations of the thermal diffusion process under controlled atmospheres with water bubbling.

were mixed and thermally treated using electrical furnace at 800 °C for 60 min with flowing various kinds of gases. To investigate the effect of moisture in the gas, a water bubbler was installed in the gas line to the furnace as shown in Figure 2. Flow meters were used to control the gas flow rates. Before entering the furnace, the gas was run through a water bubbler to create a high-humid atmosphere for humid conditions. This configuration made it possible to systematically regulate the moisture content during thermal diffusion. In this study, to indicate and optimize the ambient gas conditions for thermal diffusion process, atmospheric air (open air), dry air (dew point of −50 °C), water bubbled air, pure N_2, water bubbled N_2, and forming gas (3.8 % H_2 in N_2) were used. Here, the ZnO NPs with thermally diffused In in open air are called "ZnO:In(open-air)". Similarly, they are called "ZnO:In(dry-air)", "ZnO:In(bubbled-air)", "ZnO:In(pure-N_2)", "ZnO:In(bubbled-N_2), and "ZnO:In(H_2/N_2)", respectively. As references, as synthesized ZnO NPs without any thermal process is called "as-synthesized", and thermally treated ZnO NPs (800 °C, 60 min in open air) without In_2O_3 is called "thermally treated ZnO".

The spray-coating suspension was made by dispersing all NPs removed from furnace with 15 g of pure water. An ultrasonic homogenizer with ultrasonic technology (VCX-500) (150 W, 3 min) was used to make uniform dispersion and prevent aggregation. A centrifuge (KUBOTA 3300) (3000 rpm, 1 min) was used to settle down the large ZnO and residual In_2O_3 particles.

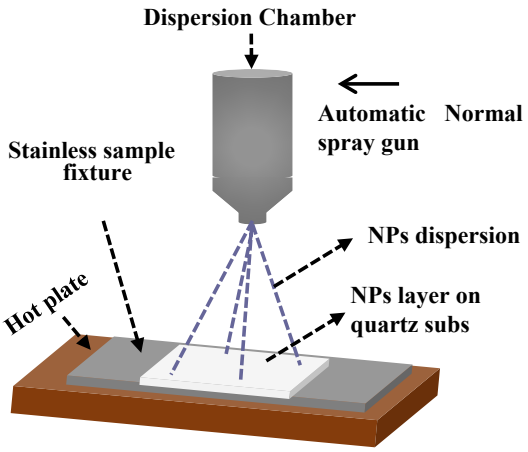

Figure 3: Illustrations of the automatic spray-coating process.

The particle sizes for as-synthesized ZnO, thermally-treated ZnO, ZnO:In(pure-N_2), ZnO:In(bubbled-N_2), ZnO:In($N_2 + H_2$), ZnO:In(bubbled-air), and ZnO:In(open-air) were found as 233, 240, 312, 252, 352, 356, and 270 nm, found from dynamic light scattering measurements (LB-500, HORIBA) in all conditions used in this study. The quartz substrate was sprayed with 7 mL of dispersion solution at 5 s of interval for nearly 15 min using an automatic spray gun and a hot plate with 500 °C as shown in Figure 3.

Sheet resistance measurements were performed at room temperature using the transfer length method with the electrodes' distance from 100 to 500 µm. The electrodes (300 µm × 300 µm square) were made by vacuum evaporated Al covered with sputtered Au.

A spectrofluorometer (FluoroMax-4, HORIBA) was used to measure PL spectra with the excitation light wavelength of 325 nm, the slit width of 3 nm, and the exposure time of 0.2 s. XRD (Smart Lab, Rigaku) with Cu Kα radiation (λ = 1.5406 Å) was used to evaluate the crystal structure, lattice parameters, and crystallite size. SEM (JCM 7000) was used to examine the surface morphology and microstructure. EDS optionally installed in SEM system was used to ascertain the constituent elements.

III. RESULTS AND DISCUSSION

SEM images of sprayed ZnO NP layers are shown in Figure 4 made of (a) as-synthesized ZnO NPs, (b) ZnO:In(pure N_2), (c) ZnO:In(open air), and (d) ZnO:In(bubbled-N_2). In all conditions, the quartz substrates were covered with ZnO NPs properly. By keeping the surface temperature high while the spraying procedure is underway, the solvent (in this case, water) quickly vaporized, decreasing the migration of ZnO-NPs resulting in suppressing the aggregation phenomena. There was no large difference among these images. From the measurements using the thickness monitor (Millimar C1200), the thickness values of NP-layers made of "as-synthesized" and "thermally-treated" ZnO NPs were 4.2 and 4.5 µm, respectively. The thickness values of other NP-layers made of ZnO:In were within the range of

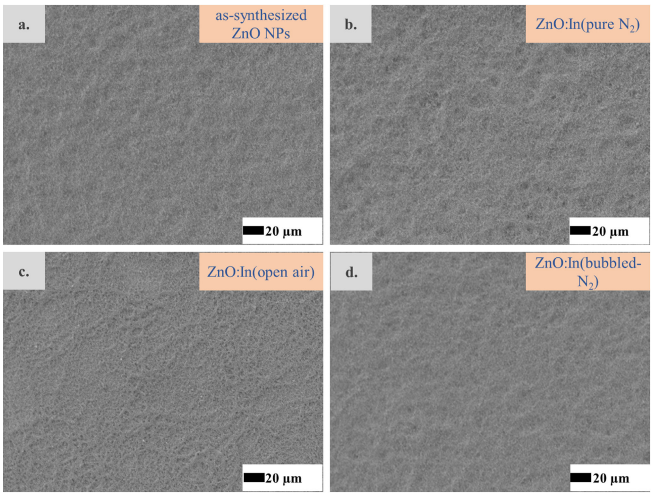

Figure 4: The SEM images of sprayed ZnO NP layers made of (a) "as-synthesized", (b) ZnO:In(pure-N_2), (c) ZnO:In(open-air), and (d) ZnO:In(bubbled-N_2).

6.0 ± 0.5 µm. A slight increase in the NP layer thickness was observed, which can be caused by the increase of NP size after the In diffusion process.

Sheet resistance behavior upon ambient gas in thermal diffusion process is shown in Figure 5(a). ZnO NP layer made of "as-synthesized" ZnO showed very high sheet resistance value in the order of $10^7\ \Omega\ sq^{-1}$. Only thermal treatment in open-air without In_2O_3 NPs ("thermally treated") had no effect on the reducing sheet resistance. ZnO NP layers made of ZnO:In NPs showed significant variation in sheet resistance depending on the ambient gases. Among these results, the sheet resistance was successfully reduced to the order of $10^5\ \Omega\ sq^{-1}$ in the condition of "ZnO:In(bubbled-N_2)". NP-layer made of "ZnO:In(open-air)" could also reach down to $10^5\ \Omega\ sq^{-1}$ order. Other conditions such as ZnO:In(pure N_2) and ZnO:In(bubbled air) also showed decrease of sheet resistance values. It is expected that the thermally diffused In affected them. On the other hand, it is interesting that the condition of "ZnO:In($H_2 + N_2$)" provided less variation, and "ZnO:In(dry air)" resulted in significant increase of sheet resistance value. These results suggested that there were factors other than simple thermal diffusion of In.

One of common conditions under which the sheet resistance decreased is the existence of moisture in the bubbled and open air. To confirm it, thermal diffusion processes were carried out using the mixture of dry-air and bubbled-air with changing the flow rate. The bubbled-air and dry-air ratios of 80:20, 50:50, and 20:80 were obtained by controlling the respective flow rates through flow meters. The values of water vapor contents were estimated by Eq. (1),

$$C_{mix} = f_{bubbled} C_{bubbled} + (1 - f_{bubbled}) C_{dry}, \quad (1)$$

where C_{mix}, $C_{bubbled}$, and C_{dry} are water vapor contents for mixed gas, bubbled-air, and dry-air, respectively, and $f_{bubbled}$ is a fraction of bubbled-air. Here, $C_{bubbled}$ can be determined as $12.8\ g\ m^{-3}$ with assuming the humidity of 100 % for

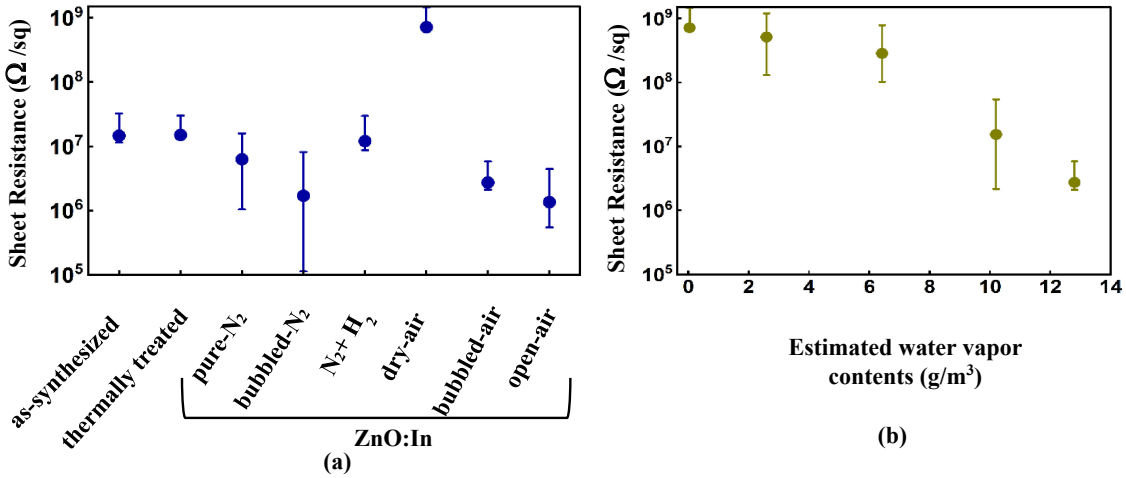

Figure 5: Sheet resistance dependence upon (a) ambient gas and (b) water vapor contents in thermal diffusion processes. Error bars indicate the distribution of experimental values and circle marks indicate the average values.

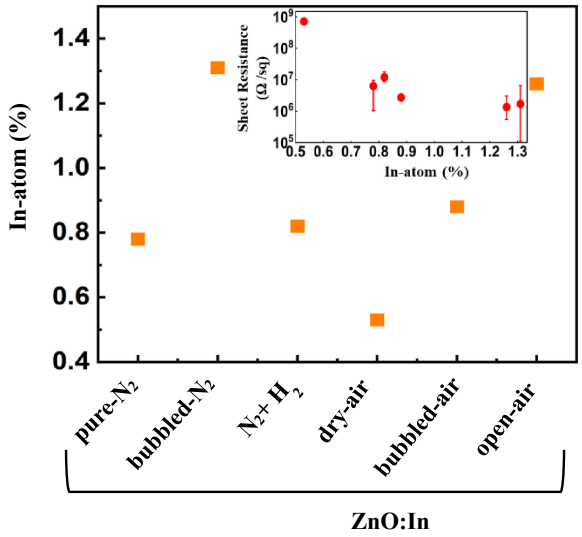

Figure 6: In-atom % variation with different gas conditions in thermal diffusion processes.

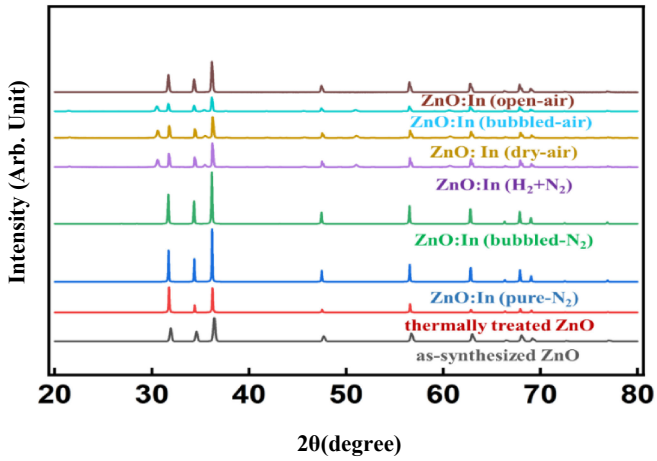

Figure 7: XRD spectra of ZnO NPs with and without thermal diffusion of In.

bubbled-air (15 °C), and C_{dry} is 0.06 g m^{-3} from the dew point of −50 °C. The resultant sheet resistance dependence upon the estimated water vapor contents is shown in Figure 5(b). The data clearly show that the sheet resistance effectively reduced with increasing the water vapor contents.

EDS results are shown in Figure 6, which were conducted on spray-coated ZnO NP layers made of ZnO:In formed in this study. Among the tested conditions, the highest incorporation of In was observed in ZnO NP layer made of ZnO:In(bubbled-N_2), which corresponds to the lowest sheet resistance value shown in Figure 5(a). Overall trend indicates that the increase of In corresponds to the decrease of sheet resistance. A correlation plot between the sheet resistance and the In concentration (derived from EDS) under various ambient conditions were included as an inset of Figure 6. Diffused In acted as donor and contributed reducing resistivity of ZnO NPs and following formed NP layers.

Figure 7 expresses the XRD results of as-synthesized ZnO NPs and various kinds of thermal treated ZnO NPs in this study. The diffraction peaks are well-described as hexagonal wurtzite structure [13, 14] with exact orientation which agrees with the standard JCPDS data [15] for ZnO. The measurements were performed on powdered samples, so there were small signals from the In_2O_3 particles before they were removed by centrifugation.

Figure 8(a) shows the variation of calculated lattice constant c values for various kinds of ZnO NPs used in this study. The lattice constant value is affected by the difference in ionic radius between the doped impurity atom (In^{3+}, 0.62 Å) and the substituted atom (Zn^{2+}, 0.60 Å). After thermal process with In_2O_3 NPs, the c value increased within the difference of the ionic radii (0.02 Å). The highest c value was obtained using "ZnO:In(bubbled-N_2)", which corresponds to the lowest sheet resistance of sprayed ZnO NP layer. And for other conditions, the trend of change in c value well corresponds to the behavior of the sheet resistance values in

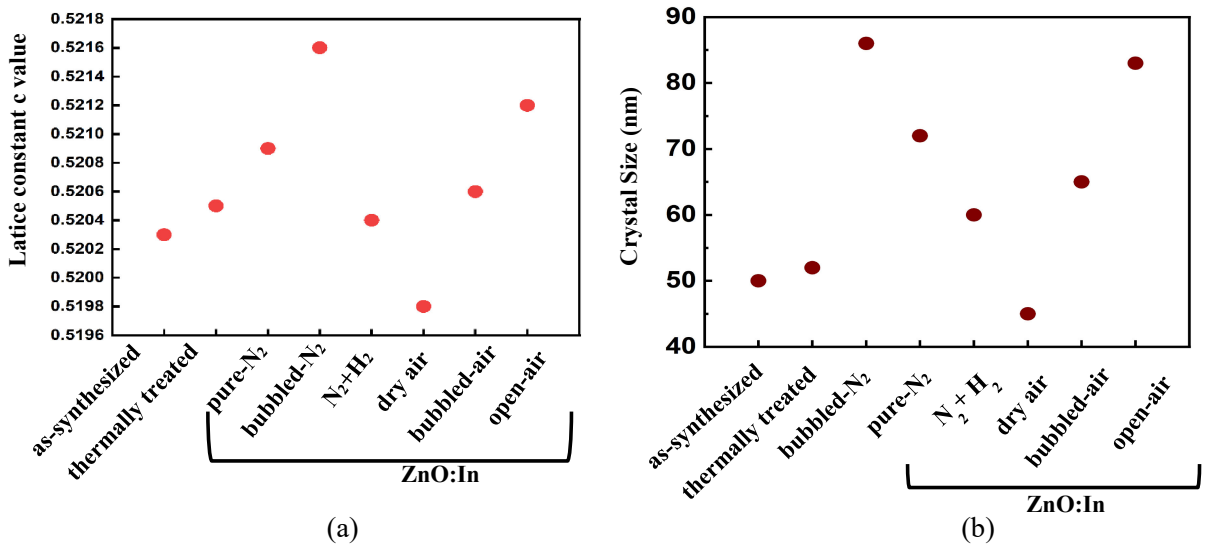

Figure 8: (a) Variation of calculated lattice constant c values and (b) estimated crystallite sizes from the Scherrer's equation.

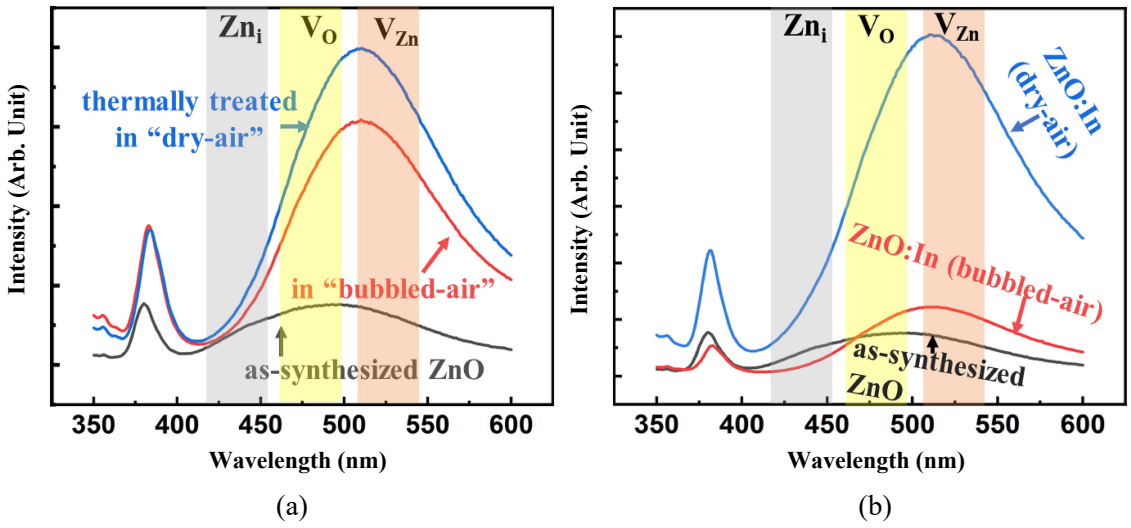

Figure 9: Variations of PL spectra of ZnO NPs by thermal treatment (a) without and (b) with In_2O_3 NPs.

Figure 5(a). It is investigated that a part of the diffused In atoms substituted for Zn atoms in the ZnO lattice.

Using Scherrer's method, based on the (100) peaks in the full-width at half maximum (FWHM) values, the crystallite size (D) was calculated using Eq. (2) [16],

$$D = \frac{0.9\lambda}{\beta \cos\theta}, \tag{2}$$

where θ is the Bragg angle of the diffraction peak, β is the FWHM in radians, and λ is the wavelength of incident X-ray. Figure 8(b) shows the calculated crystallite sizes of ZnO NPs used in this study. The largest crystallite size was obtained by "ZnO:In(bubbled-N_2)", and the variation behavior under other ambient conditions also corresponds to the variation in sheet resistance value. Grain boundaries served as carrier scattering centers, hence reducing them can improve carrier transport. However, considering the sizes of NPs of around 300 nm, the variation of the crystallite size from 45 to 86 nm cannot be expected to have a significant impact on reducing the sheet resistance value. Some literature [17] investigated that heavy In doping led the increase of the crystallite size. So, the crystallite size variation, which appears to correspond to the sheet resistance variation, seems to be caused by In doping. When In concentration increased in ZnO NPs, In concentration at the boundary of crystallites is also increased, which caused lowering of surface potential. Even in the absence of a liquid phase, crystallite coarsening can proceed via solid-state Ostwald ripening governed by surface and crystallite-boundary diffusion [18].

To confirm the effect of water vapor contents to ZnO NPs in thermal treatments, "as-synthesized" ZnO NPs were annealed without In_2O_3 NPs in dry-air and water-bubbled-air at 800 °C for 60 min. Photoluminescence spectra of sprayed ZnO NP layers using them are shown in Figure 9(a). It is clearly observed that the defects such as V_O and zinc vacancy (V_{Zn}) were increased in both dry- and water-bubbled-air. On

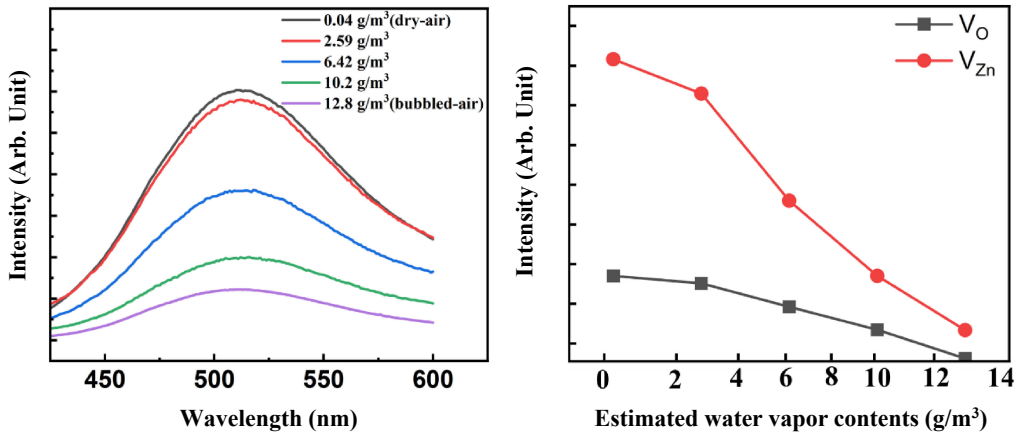

Figure 10: (a) PL spectra in defect region and (b) deconvoluted defects' area intensities under different condition of water vapor contents in In diffusion processes.

the other hand, by annealing with In_2O_3 NPs (same as In diffusion process in this study), the defects' signal was dramatically suppressed in using water-bubbled-air, while it varied less in using dry-air, as shown in Figure 9(b). For more detailed characterization, PL measurements were carried out for the samples made with intermediate water vapor contents, which corresponds to the conditions of Figure 5(b). Figure 10(a) shows the PL spectra in defect region and Figure 10(b) shows the variation of deconvoluted area intensities. It was clearly confirmed that, with increasing water vapor contents, the defect intensity decreased systematically, corresponding to the sheet resistance variation. Particularly, the decrease in V_{Zn} was dramatic.

Based on these results, there are two possible models to explain the water vapor-mediated sheet resistance reduction phenomenon. One is the passivation of V_{Zn} by OH^- and/or H^+ ions [19, 20] generated from water vapor during high temperature thermal treatment. The vacancy-type defects increase by high temperature thermal treatment in the air [21, 22], and V_{Zn} behave as deep acceptors compensating for free electrons, which is the reason why the sheet resistance value increased greatly for NP layer made of "ZnO:In(dry-air)". By terminating V_{Zn} with OH^- and/or H^+ ions, they were passivated, and the survived free electrons can contribute to decrease the sheet resistance. Another possible model is the enhanced In diffusion with water vapor in the gas (air). Previous studies have reported the formation of hydroxide states like Zn–OH and In–OH at the surface of ZnO and In_2O_3, respectively [23–25]. Especially in Ref. 25, Togashi *et al.* analyzed thermodynamically that the In–OH component could be formed by heating In_2O_3 in H_2 ambient. According to this literature, H_2O molecules from oxidized H_2 can assist the formation of In–OH, and the possibility of this reaction is enough under heating temperature of 800 °C. In our case, with increasing the water vapor contents in the gas (air), formation of In–OH was enhanced at the In_2O_3 NP surface. Basically, such hydroxyl groups are unstable and easy to be decomposed in high temperature conditions. In decomposing the Zn–OH and/or In–OH groups, the solidification occurs easily where ZnO particles and In_2O_3 particles are in contact and facilitate interfacial reactions and lattice incorporation. (This phenomenon is well described in other material cases such as Ni–Li system in Ref. 26. Similar surface reaction can occur also in our Zn–In system.) Thus, the presence of water vapor may enhance In atom diffusion and diffused In atoms can act as donors which also fill and passivate the V_{Zn}. Regarding the two explanation models mentioned above, there is no reason to rule out either one, in this stage. It is reasonable to assume that both effects exist.

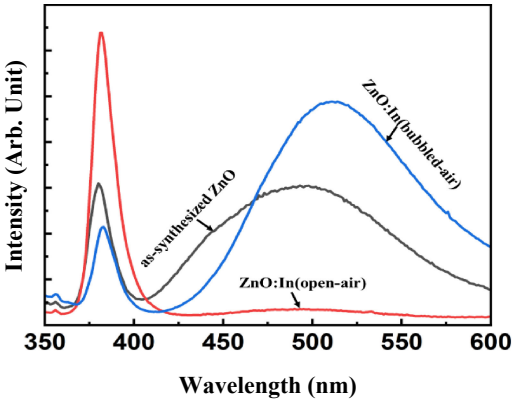

Figure 11: Comparison of PL spectra variation between ZnO:In(open-air) and ZnO:In(bubbled-air).

Finally, a PL spectrum of "ZnO:In(open-air)" is shown in Figure 11 together with the PL spectra of "as-synthesized ZnO" and "ZnO:In(bubbled-air)". This was a fortuitous discovery, but "ZnO:In(open-air)" provided the lowest sheet resistance among the air gases used in this study, and the PL measurements showed that the defects had almost completely disappeared. To confirm reproducibility, the ZnO:In(open-air) diffusion experiment conditions were made four times independently using the same processing parameters. Here, the water vapor has the property of passivating the existing V_{Zn} as mentioned above, on the other hand, it is also known to have the property of generating V_{Zn} [27, 28]. So,

the increase of water vapor content can contribute both the formation of V_{Zn} and the enhancement of In diffusion, i.e., the former increases the sheet resistance of ZnO NP layers and the latter decreases them. It needs to find the optimum conditions. In this experiment, open-air was the optimal condition for using air, the temperature of 15 °C and the humidity of 42 %, which correspond to a water vapor content of 5.38 g m^{-3}. However, from Figure 5(b), the lowest sheet resistance value cannot be obtained by using this condition. The detailed reason for this discrepancy is not cleared yet. One possible reason for this may be that the source air for "dry-air" and "open-air" was not the same ("bubbled-air" was obtained by bubbling "dry-air"). Or, it may suggest that there are other conditions besides the water vapor content. Further investigations are required.

In this study, the sheet resistance of the n-ZnO NP layer was successfully reduced to the order of $10^5\ \Omega\ \mathrm{sq}^{-1}$ by thermally diffused In doping. This value represents a marginally acceptable characteristic for application as a TFT channel layer in liquid crystal displays. Further reduction of the sheet resistance by one to two orders of magnitude, together with improvements in the stability of carrier transport properties, will be required in future work.

IV. CONCLUSION

Thermal diffusion type In-doping to ZnO NPs was achieved by thermal treatment of ZnO NPs with In_2O_3 NPs. Ambient gas during thermal treatment greatly affects the In diffusion. The presence of water vapor in particular contributed to effective In doping and a reduction in the sheet resistance of sprayed ZnO NP layers. The role of water vapor and the necessity of optimizing its contents were discussed. Two possible models such as passivation of zinc vacancy and enhancement of In diffusion with water vapor existence have been discussed.

Acknowledgments

The authors wish to acknowledge the cooperation of Center for Integrated Research in Science, Shimane University, for providing the XRD measurement system and SNCC for providing the automatic spray gun, SEM, and EDS systems. This work was supported by JSPS KAKENHI Grant No. 20K05327.

References

[1] S. Roncallo, J. D. Painter, M. A. Cousins, D. W. Lane, and K. D. Rogers, Thin Solid Films **516**, 8493 (2008).
[2] M. Dehghan and A. Behjat, RSC Adv. **9**, 20917 (2019).
[3] J. K. Saha, R. N. Bukke, N. N. Mude, and J. Jang, Sci. Rep. **10**, 8999 (2020).
[4] F. F. Vidor, G. I. Wirth, and U. Hilleringmann, Microelectron. Reliab. **54**, 2760 (2014).
[5] M. Kimura, Jpn. J. Appl. Phys. **58**, 090503 (2019).
[6] K. Waszkowska, O. Krupka, O. Kharchenko, V. Figà, V. Smokal, N. Kutsevol, and B. Sahraoui, Appl. Nanosci. **10**, 4977 (2020).
[7] I. M. Shafiqul, R. Deep, J. Lin, T. Yoshida, and Y. Fujita, Phys. Status Solidi Rapid Res. Lett. **16**, 2100556 (2022).
[8] M. M. Islam, T. Yoshida, and Y. Fujita, Coatings **12**, 57 (2022).
[9] A. N. Mallika, A. RamachandraReddy, K. SowriBabu, and K. V. Reddy, Ceram. Int. **40**, 12171 (2014).
[10] M.-S. Oh, D.-K. Hwang, D.-J. Seong, H.-S. Hwang, S.-J. Park, and E. D. Kim, J. Electrochem. Soc. **155**, D599 (2008).
[11] N. Ito, Y. Sato, P. K. Song, A. Kaijio, K. Inoue, and Y. Shigesato, Thin Solid Films **496**, 99 (2006).
[12] K. Senthilkumar, O. Senthilkumar, S. Morito, T. Ohba, and Y. Fujita, J. Nanopart. Res. **14**, 1205 (2012).
[13] T.-H. Chen and T.-Y. Liao, J. Nanomater. **2013**, 502382 (2013).
[14] Z.-Z. Li, Z.-Z. Chen, W. Huang, S.-H. Chang, and X.-M. Ma, Appl. Surf. Sci. **257**, 8486 (2011).
[15] K. Pradeev Raj, K. Sadaiyandi, A. Kennedy, and R. Thamizselvi, Mater. Chem. Phys. **183**, 24 (2016).
[16] B. N. Q. Trinh, T. D. Chien, N. Q. Hoa, and D. H. Minh, J. Sci. Adv. Mater. Devices **5**, 497 (2020).
[17] S. Mourad, J. El Ghoul, K. Omri, and K. Khirouni, Chin. Phys. B **28**, 047701 (2019).
[18] H. Wang, Y. Liu, Y. Xie, J. Ma, D. Han, and S. Sang, Chemosensors **13**, 239 (2025).
[19] Z. Wang, H. Gao, D. Wu, J. Meng, J. Deng, and M. Cui, Molecules **29**, 2104 (2024).
[20] A. Kumar, D. K. Gorai, and M. I. Ahmad, J. Mater. Sci.: Mater. Electron. **34**, 426 (2023).
[21] A. K. Abisheva, D. A. Afanasyev, B. R. Ilyassov, A. K. Aimukhanov, V. A. Kulbachinskii, and A. K. Zeinidenov, Physica E **159**, 115932 (2024).
[22] T.-B. Hur, G. S. Jeen, Y.-H. Hwang, and H.-K. Kim, J. Appl. Phys. **94**, 5787 (2003).
[23] M. Valtiner, S. Borodin, and G. Grundmeier, Phys. Chem. Chem. Phys. **9**, 2406 (2007).
[24] M. Wagner, P. Lackner, S. Seiler, A. Brunsch, R. Bliem, S. Gerhold, Z. Wang, J. Osiecki, K. Schulte, L. A. Boatner, M. Schmid, B. Meyer, and U. Diebold, ACS Nano **11**, 11531 (2017).
[25] R. Togashi, Y. Kisanuki, K. Goto, H. Murakami, A. Kuramata, S. Yamakoshi, B. Monemar, A. Koukitu, and Y. Kumagai, Jpn. J. Appl. Phys. **55**, 1202BE (2016).
[26] A. Tayal, P. Barai, H. Zhong, O. Kahvecioglu, X. Wang, K. Z. Pupek, L. Ma, S. N. Ehrlich, V. Srinivasan, X. Qu, J. Bai, and F. Wang, Adv. Mater. **36**, 2312027 (2024).
[27] T. T. John, K. R. Priolkar, A. Bessière, P. R. Sarode, and B. Viana, J. Phys. Chem. C **115**, 18070 (2011).
[28] X. Song, M. Schrade, N. Masó, and T. G. Finstad, J. Alloys Compd. **710**, 762 (2017).